https://doi.org/10.5194/egusphere-2025-6461
Preprint. Discussion started: 19 January 2026

Constraining the atmospheric hydrogen oxidation and soil sinks using HFC-152a

Kane Stone[1], Candice Chen[1], Susan Solomon[1], Luke M. Western[2], Paul B. Krummel[3], Gabrielle Pétron[4,5], Jens Mühle[6], and Simon O'Doherty[7]

[1]Department of Earth Atmospheric and Planetary Sciences, Massachusetts Institute of Technology, Cambridge, MA, United States

[2]Center for Sustainability Science and Strategy, Massachusetts Institute of Technology, Cambridge, MA, United States

[3]CSIRO Environment, Aspendale, Victoria, Australia

[4]Cooperative Institute for Research in Environmental Sciences, University of Colorado Boulder, Boulder, USA

[5]NOAA Global Monitoring Laboratory, Boulder, USA

[6]Scripps Institution of Oceanography, University of California San Diego, La Jolla, CA, USA

[7]School of Chemistry, University of Bristol, Bristol, UK

Correspondence to: Kane Stone (stonek@mit.edu)

Abstract. As the hydrogen (H_2) economy expands, there is growing interest in understanding the atmospheric lifetime of H_2, which affects its impact on atmospheric chemistry and climate. While some global H_2 is destroyed via reaction with the hydroxyl radical (OH), most is lost to microbial activity in soils. However, the sources and sinks of H_2 are still uncertain on global and local scales. This study focuses on how monthly resolved observations of HFC-152a can help to constrain the seasonal OH cycle and the H_2 budget, particularly the seasonal range and phase of H_2 oxidation and soil loss. Seasonal observations of HFC-152a are used to constrain OH through a Bayesian inversion in a three-box model comprising the Northern, Tropics, and Southern regions over 2010–2022. In the North, a seasonal range of the soil sink of 18–21 ± 8 Tg year^{-1} is found, peaking in July–August, while the OH loss seasonal range is 8 ± 1 Tg year^{-1}, peaking in July. The South has much less land and so displays a smaller soil sink seasonal range of 2–3 ± 2.5 Tg year^{-1}, peaking in January–March. The OH loss in the South has a seasonal range of 7 ± 1 Tg year^{-1}, peaking in January. The OH and soil sink loss in the Tropics is more consistent across all months, but with larger uncertainty. The results presented here will be a useful comparison for H_2 cycles in fully integrated chemistry climate models.

1. Introduction

There has been a growing interest in using hydrogen (H_2) as an alternative to fossil fuels (Hydrogen Council, 2020; IEA, 2023). H_2 itself is not a greenhouse gas; however, its main atmospheric sink is through reaction with the hydroxyl radical (OH),

https://doi.org/10.5194/egusphere-2025-6461
Preprint. Discussion started: 19 January 2026

which in turn affects three major greenhouse gases: methane, tropospheric ozone, and stratospheric water vapor. Therefore, H_2 is an indirect greenhouse gas, with a net 100-year global warming potential (GWP) of around 8–12 (6–16 when including uncertainties) (Bertagni et al., 2022; Chen et al., 2024; Derwent, 2023; Ouyang et al., 2025a; Warwick et al., 2023). As shown in the above studies, the rate of loss of hydrogen to soil is both large and highly uncertain and therefore dominates the uncertainty in this important GWP. With future emissions likely to increase as the H_2 economy increases, it is important to better understand the sinks of H_2.

The primary source of H_2 in the atmosphere is oxidation of methane and volatile organic compounds (VOCs) such as isoprene into formaldehyde (CH_2O), which then photolyzes to form H_2. H_2 can also be produced from combustion in auto engines. Overall, global anthropogenic emissions have likely been decreasing due to better air quality controls (Paulot et al., 2021). Biomass burning is another major source of H_2 emissions (Crutzen et al., 1979), with large events coinciding with El Niño (Duncan et al., 2003). Hydrogen is leakage-prone from infrastructure. Therefore, if the H_2 economy were to increase in the future, this will also likely increase emissions and the atmospheric concentration of H_2 (Esquivel-Elizondo et al., 2023).

Atmospheric H_2 has a lifetime of ~2 years resulting from two main sinks. The smaller of the two sinks is reaction with atmospheric OH, which is estimated to account for an approximate loss of 15–20 Tg year^{-1} (Ehhalt and Rohrer, 2013; Hauglustaine and Ehhalt, 2002; Novelli et al., 1999; Paulot et al., 2021; Sanderson et al., 2003; Yashiro et al., 2011). However, uncertainty remains in the impact of OH on H_2 and its subsequent impact on greenhouse gases due to model biases of OH, which typically overestimate the OH abundance (e.g. Yang et al., 2025).

The major sink of H_2 is through microbial driven near-surface soil uptake (Conrad et al., 1983), which predominantly occurs in the Northern Hemisphere. This results in a greater concentration of H_2 in the tropics and Southern Hemisphere as seen from the National Oceanic and Atmospheric Administration (NOAA) global surface air sampling network (Novelli et al., 1999; Pétron et al., 2024). Soil uptake is also largely dependent on soil moisture and temperature, and therefore is expected to have a strong seasonality in the Northern Hemisphere, likely peaking in the late summer/early autumn (Bertagni et al., 2021; Ehhalt and Rohrer, 2009; Reji et al., 2025; Yonemura et al., 1999). However, large uncertainties in the global and hemispherical loss due to soils remain, with published estimates ranging from ~50–88 Tg year^{-1}. For example, Rhee et al. (2006) used measurements of stable isotopic ratios of H_2 to infer a global soil sink of 88 Tg year^{-1}, accounting for over 80 % of the total loss. Modelling studies that incorporate a moisture-based soil sink typically obtain lower values of ~55 Tg year^{-1} (e.g. Brown et al., 2025a; Paulot et al., 2021; Pieterse et al., 2013) that peak between June–August depending on the model (Brown et al., 2025b). A recent model and observations synthesis of the H_2 budget arrives at a global soil sink of 50 ± 18 Tg year^{-1} (Ouyang et al., 2025a). Most current global climate models do not incorporate an interactive soil sink (e.g. Sand et al., 2023).

Methyl chloroform (CH_3CCl_3, MCF) has, in the past, been used as the main reference gas to obtain the oxidative capacity of the atmosphere (Montzka et al., 2011; Naus et al., 2021; Patra et al., 2021; Prinn et al., 1992). When emissions of MCF were relatively well known, the retrieved uncertainty of mean tropospheric OH was fairly well constrained. But MCF is an ozone depleting substance and therefore production and consumption have been completely phased out since 2015 under the Montreal Protocol and its subsequent amendments. This resulted in near zero emissions and its global abundance dropping to very low levels and therefore increased uncertainty in the measured MCF values and derived OH due for example to limits on instrument precision. A search for other viable candidates to constrain global mean OH is underway, with hydrofluorocarbons (HFCs) being a top contender (Liang et al., 2017; Thompson et al., 2024).

Here, the short-lived man-made gas HFC-152a is used to obtain information of the OH seasonality in a 3-box atmospheric model through an optimal estimation, similar to previous work using MCF (Bousquet et al., 2005). HFC-152a has been shown to be a viable alternative to MCF (Liang et al., 2017). The main loss pathway of HFC-152a is through OH oxidation, with a short OH lifetime of 1.55 years (e.g. Burkholder and Hondnebrog, 2023). There is also a much smaller stratospheric sink with a lifetime of 44.3 years. Emissions of HFC-152a are not well constrained (Simmonds et al., 2016; Western et al., 2025), which limits the ability to retrieve absolute OH values, however, HFC-152a emissions are not expected to vary seasonally, therefore, the short OH lifetime of HFC-152a allows for higher accuracy of seasonal anomalies (derived as a difference from the yearly mean) of OH to be retrieved in this study; this information is then used to constrain the seasonal retrieval of the H_2 OH and soil sink yearly ranges (maximum – minimum) and phases. Absolute H_2 budget terms and overall lifetimes are not presented in this study because the absolute values of the retrieved OH are not constrained by our approach.

The next section describes the methods, observational data, and model data used in the study. This is followed by results presenting initial forward model calculation and retrieval fits of HFC-152a and H_2. This is followed by retrieved OH and H_2 oxidation rate anomalies averaged over 2010–2022 (2010 being the earliest start date that includes all observational sites). H_2 soil sink anomalies over the same period are then presented and discussed for each box. Conclusions are summarized in the last section.

2. Methods and Data

2.1 Box model

An equal mass three-box tropospheric model is constructed to act as the forward model in the retrieval and uses the same box boundaries as Chen et al. (2024). The box boundaries constitute the South (90°–20° S), Tropics (20° S–20° N), and North (20°–90° N) regions. Transport between the boxes is based on diffusive transport terms from (Cunnold et al., 1994), with modifications to account for different box boundaries and to ensure a realistic North-South gradient constrained by observations of the long-lived tracer, SF_6 from the Advanced Global Atmospheric Gas Experiment (AGAGE) (Prinn et al., 2025, 2018). The box model steps daily in time, and gas phase oxidation of HFC-152a and H_2 are calculated using ERA5 monthly temperatures, averaged from the surface up to 200 hPa for each box (Hersbach et al., 2020). Transport and temperature terms used in the box model are shown in Table S1. The Arrhenius equations used for the HFC-152a and H_2 oxidation reactions are from (Burkholder et al., 2019) and are also shown in the supplement.

2.2 Observations and forward model parameters

HFC-152a is used in the model to obtain the monthly resolved OH concentration of each box over 2010–2022. HFC-152a has a very short OH lifetime of 1.5–1.6 years (Ko et al., 2013, Simmonds et al., 2016), allowing for the OH seasonal cycle to be derived from the measurements. It has been shown to be suitable for retrieving global average OH (Liang et al., 2017; Thompson et al., 2024). Monthly means of HFC-152a are derived from dry air mole fraction measurements at three AGAGE background sites (Prinn et al., 2025). The three representative sites used for each box in our model are: South box, Kennaook/Cape Grim (CGO, Australia, 40.7° S); Tropics box, Cape Matatula (SMO, American Samoa, 14° S); North box, Mace Head (MHD, Ireland, 53.3° N). A second Tropical location at Ragged Point (RPB, Barbados, 13.2° N) that has higher mole fractions than SMO was not used as it has more frequent intrusions of extra-tropical air. Instead, a 20 % increase offset has been applied to the SMO data. H_2 observations used here come from AGAGE in situ measurements at CGO and MHD for the South and North boxes respectively and NOAA weekly flask measurements averaged over three stations: Ascension Island (United Kingdom, 8° S), Cape Matatula (American Samoa, 14°S), and Mahe Island (Seychelles, 4.6° S) (Pétron et al., 2024, 2025). Both AGAGE and NOAA datasets are on the MPI-2009 calibration scale. A comparison of the two AGAGE stations that make H_2 measurements (MHD and CGO) with a zonally and temporally resolved background air H_2 distribution based on the NOAA flask data is shown in Fig. S1. In the South and North boxes, the two datasets are in excellent agreement, improving confidence that the single AGAGE station within each box gives a good representation of the entire box. For the Tropics box, the average H_2 time series of the three NOAA stations listed above is also shown. Also, see Fig. S1 for the latitudinal distribution of the AGAGE stations and NOAA sites used in this study.

Emissions estimates for HFC-152a are taken from the Emission Database for Global Atmospheric Research (EDGAR: version EDGAR_2025_GHG) yearly emissions gridded dataset (Crippa et al., 2025). The data are supplied as annual grid map emissions, and it is assumed that the HFC-152a emissions do not vary over the course of a year in this study. There are differences between EDGAR emissions of HFC-152a and other emissions datasets (e.g. Western et al., 2025), and recent inversions (e.g. Thompson et al., 2024). Thus, the uncertainty in these emissions is reflected in the prior uncertainty value chosen for HFC-152a emissions of 15% as described below.

Prior information for the seasonal amplitude of OH is taken from Spivakovsky et al. (2000) and scaled to match a global tropospheric OH concentration of $1x10^6$ molecules cm^{-3}, in line with previous literature indicating a global tropospheric oxidative capacity between $0.9–1.0x10^6$ molecules cm^{-3} (Lawrence and Jockel, 2001). However, it is important to note that some studies suggest a global abundance of OH as high as $1.13x10^6$ molecules cm^{-3} (Liang et al., 2017). As the HFC-152a emissions are not well constrained, the choice of OH prior concentration will influence the optimized OH values, but much less so the amplitude of the OH seasonal cycle in the North and South boxes, where HFC-152a has large seasonal cycles. This was confirmed by comparing optimized seasonal ranges of OH using three prior OH global mean values of 0.9 x10^{6} molecules cm^{-3}, 1.0 x10^{6} molecules cm^{-3}, and 1.1 x10^{6} molecules cm^{-3}, which shows virtually no sensitivity to the prescribed OH global mean value in the North and South boxes (see Fig. S2).

H_2 direct emissions data include biomass burning, anthropogenic, and nitrogen fixation emissions. Anthropogenic emissions of H_2 use H_2 to carbon monoxide (CO) emission factors (see Ehhalt and Rohrer, 2009; Paulot et al., 2021). These emissions factors are used to estimate H_2 emissions from different anthropogenic sources of CO from the current CMIP7 emissions dataset (these include inputs for residential, commercial, transportation, and shipping sources (Feng et al., 2020; Hoesly et al., 2025) for the 2010–2022 study period. Biomass burning emissions of H_2 from CMIP7 are directly available (van Marle et al., 2017; van Marle and Werf, 2025), so no conversion factor is needed. Anthropogenic emissions of CO, and therefore H_2, have likely been declining since 1990 due to stricter regulations of combustion emissions by vehicles (catalytic converter) and industrial processes (e.g. Ouyang et al., 2025b). However, not all emissions of H_2 are contiguous with CO (Paulot et al., 2025), and therefore large uncertainty in emissions, and emission sources remain. Emissions from nitrogen fixation are also included in the model, totaling 9 Tg year^{-1} globally following Paulot et al. (2021). Global and individual box emissions of H_2 used in the forward model are shown in Fig. 1. The other major source of H_2 in the atmosphere is chemical production through a two-step process beginning with the oxidation of methane and VOCs to CH_2O, which then photolyzes into H_2. H_2 chemical production values are derived in two ways: 1) Using the specified dynamics version of the Whole Atmosphere Chemistry Climate Model (WACCM6) (Gettelman et al., 2019) photolysis rates of CH_2O from 975 hPa to 200 hPa for the Tropics box and up to 300 hPa for the North and South boxes. To account for any potential biases in the WACCM CH_2O, a scaling factor representing the difference between WACCM and the Tropospheric Ozone and its Precursors (TROPESS) CH_2O reanalysis seasonal amplitude was applied (Miyazaki et al., 2020). 2) Using the pseudo-linear OH-CH_2O relationship as described in Wolfe et al. (2019) to obtain H_2 chemical production rates from optimized OH:

$$j_{CH_2Ob}[CH_2O] = j_{CH_2Ob}\frac{\alpha k'_{OH}[OH] + P_0}{j_{CH_2Oa} + j_{CH_2Ob} + k_{CH_2O+OH}[OH]} \tag{1}$$

Where $\alpha k'_{OH}[OH]$ describes the production of CH_2O through hydrocarbon oxidation, P_0 represents production from non-OH sources. j_{CH2Oa} and j_{CH2Ob} are the CH_2O photolysis frequencies, and $k_{CH2O+OH}$ is the CH_2O oxidation rate constant. Slope ($\alpha k'_{OH}[OH]$) and intercept (P0) terms for each box are derived from TROPESS OH and CH_2O concentrations and from WACCM photolysis frequencies averaged over the same regions as method 1 and are shown in Fig. S3. The pseudo-linear relationship stems from the photolysis loss of CH_2O being greater than the production coming from oxidation of long-lived hydrocarbons, such as CH_4. However, this is likely not always the case in all regions and therefore should be treated as an approximation only, especially in the Tropics box as can be seen by the limited linear fit in Fig. S3. A constant prior soil sink was used in each box for the entire period to approximately close the H_2 budget.

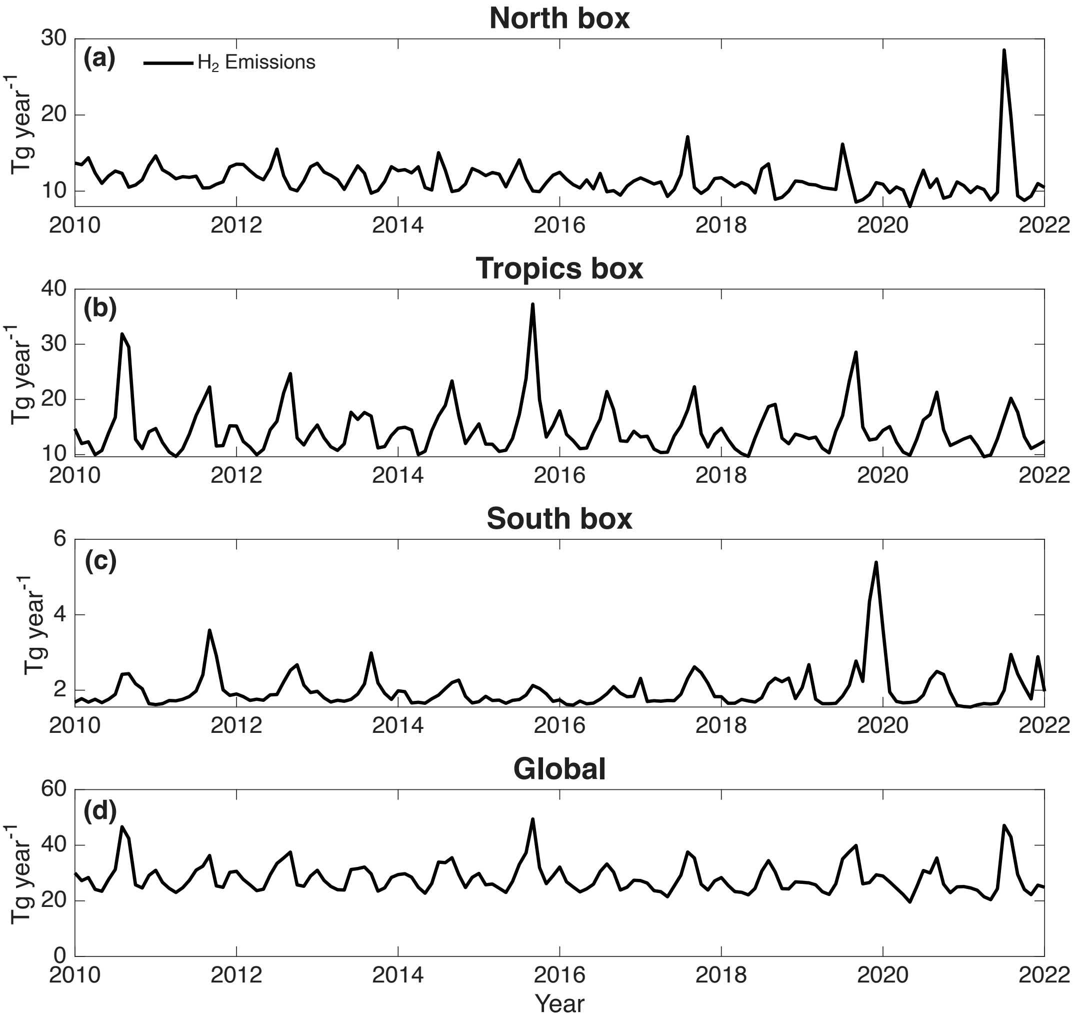

Figure 1. 2010–2022 monthly prior emissions of H_2 used in the prior forward model calculation for the (a) North box, (b) Tropics box, (c) South box, and (d) globally.

155 2.3 Inversion model

The inversion model used in this study is a Bayesian optimal estimator (Rodgers, 2000). The model optimizes monthly OH and yearly emissions for HFC-152a, as well as the monthly H_2 soil sink, emissions, and chemical production rates. The retrieved state vector is obtained by solving the following equation iteratively,

$$x_{i+1} = x_a + S_a K_i^T (K_i S_a K_i^T + S_e)^{-1} (y - F(x_i) + K_i(x_i - x_a)) \quad (2)$$

160 Where, for iteration *i*+1, x_a is the prior state vector, S_a is the prior error covariance matrix, K_i is the Jacobian from the previous iteration, S_e is the observational error covariance matrix, y are the observations, F is the forward model and x_i is the state vector

from the previous iteration. The retrieval is run until convergence, determined by minimizing the following form of the cost function from Equation 5.33 in Rodgers (2000),

$$d_i^2 = \left(F(x_{i+1}) - F(x_i)\right)^T S_{\delta y}^{-1}\left(F(x_{i+1}) - F(x_i)\right) \ll m \tag{3}$$

165 Where $S_{\delta y}^{-1}$ is the inverse of covariance of the difference between the fit and the measurements, and m is the number of observational constraints.

Table 1. Prior uncertainties, as percents of absolute values, used in all optimized configurations.

Case name	OH uncertainty	HFC-152a emission uncertainty	H_2 emission uncertainty	Soil sink uncertainty	Chemical production uncertainty
35 % uncertainty	35	15	35	35	35
15 % uncertainty	35	15	15	35	15
55 % uncertainty	35	15	55	35	55
CH_2O derived from OH	35	15	35	35	-

HFC-152a emissions uncertainty was set to 15%, and OH uncertainty was set to 35%. These values were obtained through an 170 L-curve optimization to ensure the prior uncertainties values minimized retrieval uncertainties while avoiding overfitting (see Fig. S4). Considering that OH and CH_2O are strongly correlated, both methods in determining chemical production, as described in section 2.2, are used in separate optimizations. When model values of CH_2O photolysis rates are used directly, chemical production is also retrieved with cross-correlation between OH established in the prior covariance to ensure correct chemical production seasonality. When chemical production values are derived using Eq. 1, they are not optimized but 175 calculated after each iteration in Eq. 2. Four retrievals are then performed to test the sensitivity of the soil sink amplitude on different setups: 1) using model values for chemical production with a prior uncertainty of 35 %, the same as OH, and H_2 emission uncertainty is also set to 35 %, 2) same as 1) but chemical production and H_2 emissions uncertainties set to 15 %, 3) Same as 1) but chemical production and H_2 emissions uncertainties set to 55 %, 4) using retrieved OH to derive chemical production following Eq. 1, and H_2 emission uncertainty is set to 35 %. Case setups are summarized in Table 1.

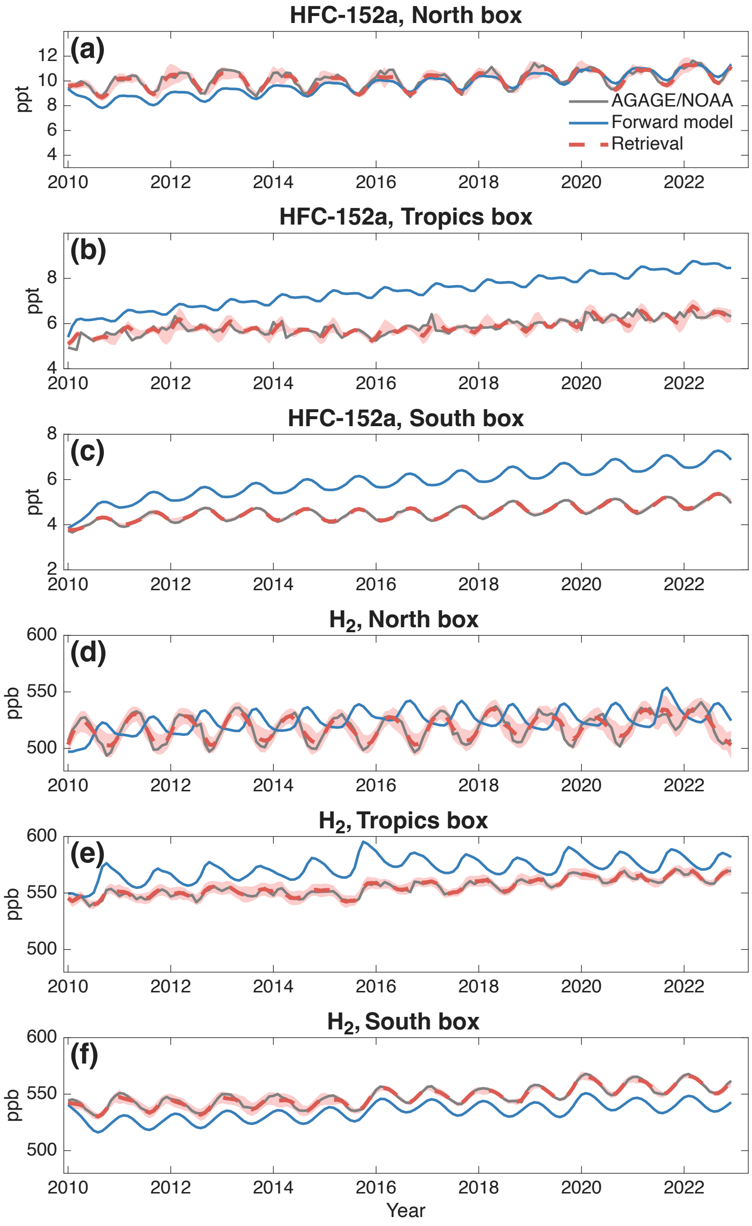

180

Figure 2. Comparison of the forward model (blue line), observations (gray line), and the retrieval fit (dashed red line) of HFC-152a and H_2 over 2010–2022. HFC-152a for the North box (20°–90° N), Tropics box (20° S–20° N), and South box (20°–90° S) are shown in panels a, b, and c respectively. Similarly, for H_2 in panels d, e, and f. The retrieved fit is shown for the 35 % prior uncertainty case along with the posterior standard deviation (shaded region). For the North and South boxes, AGAGE data is used for both HFC-152a and H_2. For the Tropics box, AGAGE Cape Matatula data is used for HFC-152a, and NOAA data is used for H_2 (see methods).

Prior emission values for HFC-152a are expected to be correlated in time for each box, therefore an exponential correlation function is used with a temporal correlation length of 5 years, similar to Thompson et al. (2024). A temporal correlation of 12 months was applied to H_2 emissions. This is much shorter than HFC-152a, as H_2 emissions are strongly dependent on seasonal biomass burning emissions. OH values are not expected to be correlated in time. Marginal posterior standard deviation uncertainties are obtained from the square root of the diagonal terms of the posterior covariance matrix, S, which is defined as,

$$S = S_a - S_a K^T (S_e + K S_a K^T)^{-1} K S_a \tag{4}$$

3 Result and discussion

3.1 Forward model and retrieved fits to observations

AGAGE and NOAA dry air mole fractions of HFC-152a and H_2 representing the “observed” means for the 3 model boxes are shown in Fig. 2. The modeled prior and retrieval posterior means are also shown. For HFC-152a, the major source of the seasonality in the North and South boxes is governed by loss to OH (also see Fig. 3), and therefore the North and South boxes have seasonality that is clearly out of phase and is well captured by the forward model. In the Tropics box, there is little observed seasonality and variability of HFC-152a. The forward model does show repeated small amplitude double peaked seasonality that is due primarily to the double peak tropical OH prior mean and transport between boxes (See Fig. 2b). The differences in observed and modeled trends in HFC-152a are likely due to uncertainties in emissions estimates. Indeed, retrieved global emissions estimates for HFC-152a have a smaller yearly growth than the EDGAR emissions used in this study (see Fig. S5). This is in agreement with year-year changes from Thompson et al. (2024) and Western et al. (2025), with small differences in absolute values that are within retrieved uncertainties between the studies (not shown). Transport parameters between boxes used in the model can also influence individual box trends and are a source of uncertainty in this three-box model setup. The HFC-152a time series modelled using the retrieved emissions and OH values agree very well with the observations in all boxes with only slight discrepancies in sharp peaks in the observations, for example in 2018 in the North box.

Observed mole fractions of H_2 also show obvious seasonality in both the North and South boxes. In the North box, the seasonality peaks around May and valleys around October. The main driver of this seasonal phase is very likely the soil sink (Fig. 2d). This is clear (and shown later in Fig. 4) when comparing to the forward model H_2 calculation that has a constant soil sink, which exhibits a seasonality that is 9 months out of phase compared to the observations. It is therefore evident that the soil sink has a large seasonal range and plays a major role in governing the seasonality of H_2 in the Northern Hemisphere.

In the Tropics Box, the seasonal variability in the observations of H_2 is mostly controlled by biomass burning and chemical production, with larger changes occurring during years of larger biomass burning, such as in 2016 and 2020 (See Fig. S6). The large biomass burning emissions, in combination with an increasing trend in CH_2O results in observed step changes in H_2 in the Tropics and South Box (Pétron et al., 2024).

In contrast to the North box, in the South box, the forward model seasonality in the H_2 mole fraction is in good agreement with the observations. This is due to the seasonality in the Southern Hemisphere being less dependent on the soil sink than in the North box. Similar to the Tropics box, the Southern Hemisphere observations display a stepped increase in both 2016 and 2020 due to biomass burning that is captured well in the forward model. The initial agreement of the forward modelled mole fractions with observations in all boxes gives confidence that the prior values used here are a reasonable estimation of the competing sources and sinks in each box. The time series of H_2 modelled using the retrieved sources and sinks agree very well with the observations in all boxes.

3.2 Retrieval of OH

Monthly averaged prior mean and retrieved OH anomalies are shown in Figs. 3a, 3c, 3e, and 3g for the North box, Tropics box, South box, and globally, respectively for two cases (the 35 % prior uncertainty case and the CH_2O derived from OH case). The differences between retrieved OH anomalies are small between the 2 cases. Error bars show the posterior standard deviations for the 35 % uncertainty inversion case.

In the North box, the mean retrieved OH range is 16–17 $\times10^5$ molecules cm^{-3}, peaking in June–July, with a posterior standard deviation of 2.5×10^5 molecules cm^{-3}. The retrieved values have a higher and sharper peak than the prior mean with a difference in range of ~6.0×10^5 molecules cm^{-3}. The seasonal range of values are in good agreement with previous work for the Northern Hemisphere (Bousquet et al., 2005). This results in a peak H_2 oxidative loss occurring in June–July with a seasonal range of 8.0 Tg $year^{-1}$ and a posterior standard deviation of 1 Tg $year^{-1}$ (Fig. 3b).

In the Tropics (Figs. 3c, and 3d), the retrieved OH seasonal range is much smaller, at ~0.5×10^5, compared to the North box. A peak OH value is retrieved in February–March. However, as the seasonal signals of HFC-152a observations in the tropics are less consistent year-to-year compared to the North and South boxes, the Tropics box retrieval is more sensitive to changes in initial OH and transport conditions (See Fig. 2 and Fig. S2). This results in a yearly range in H_2 loss of 4 Tg $year^{-1}$ with a posterior standard deviation of 2.5 Tg $year^{-1}$.

The South box has a lower retrieved OH range compared to the North box, at 13×10^5 molecules cm^{-3}, peaking in December–January. These lower values, along with the slightly lower temperatures in the South box result in a retrieved range of H_2 oxidative loss of 7 Tg $year^{-1}$ and a retrieved uncertainty of 1 Tg $year^{-1}$. Overall, the optimized global OH concentration and H_2 oxidative loss is consistent over the year (Fig. 3g).

https://doi.org/10.5194/egusphere-2025-6461
Preprint. Discussion started: 19 January 2026

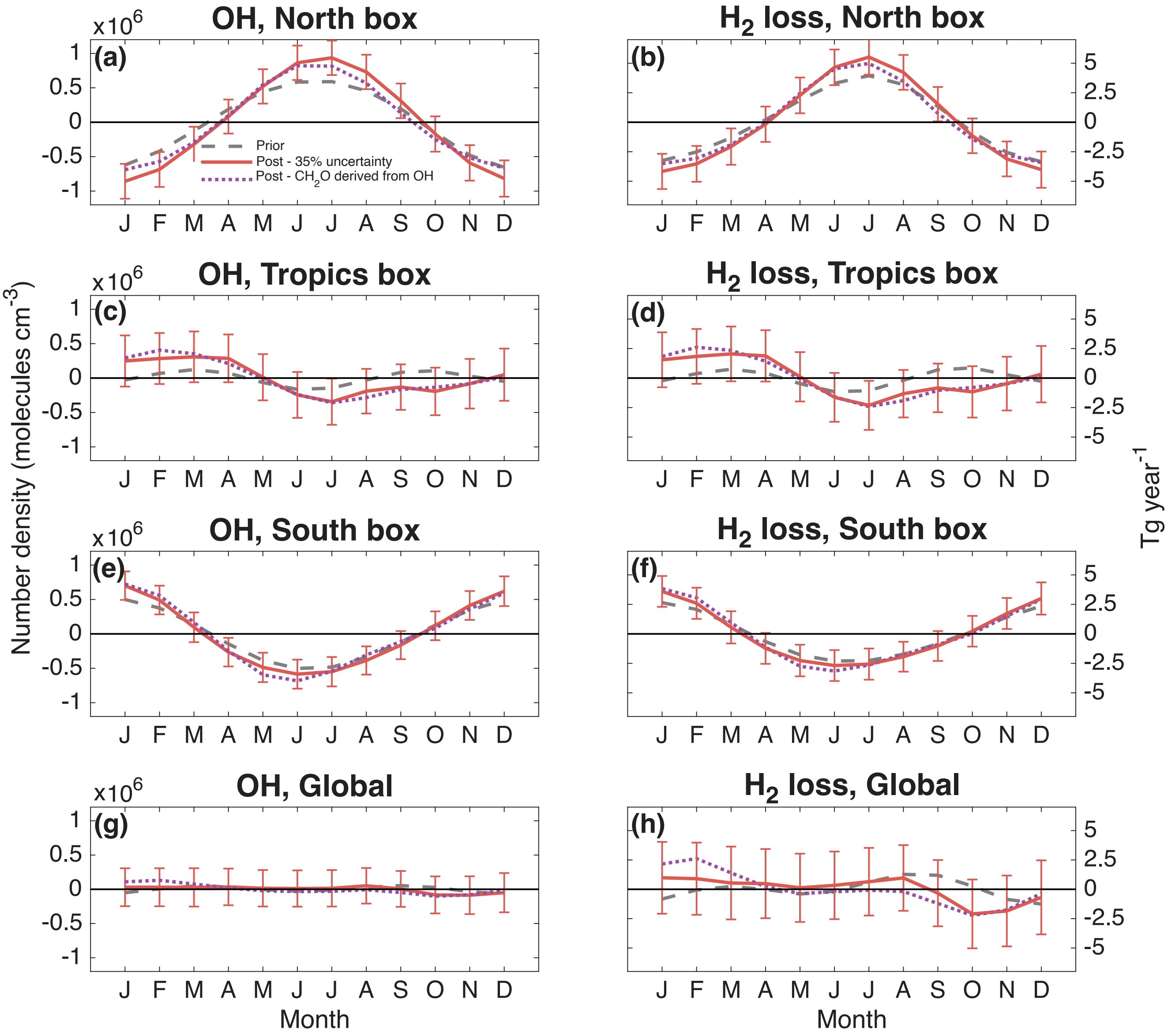

245

Figure 3. Monthly prior and retrieved mean anomalies for OH concentrations and H$_2$ oxidative loss rates for the (a, b) North box, (b, c) Tropics box, (d, e) South box, and (g, h) globally. The error bars show the retrieved posterior standard deviations calculated from the posterior covariance. The retrieved values are shown for the 35 % uncertainty and the CH$_2$O derived from OH cases. Monthly average values are taken from data over 2010–2022.

250

3.3 Retrieval of the soil sink

Fig. 4 shows the soil sink retrieval for all inversion cases (see methods). Posterior standard deviation uncertainties are shown for the 35 % uncertainty and the CH_2O derived from OH cases as error bars. The range in the retrieval means for the 15 %, 35 %, and 55 % uncertainty cases is shown as the shaded area, which is less than half of the 1-standard deviation uncertainty for a single case. It is important to emphasize that the prior soil sink is constant over the course of a year, so that the seasonal information that is retrieved is not constrained to the choice of prior and is hence a key finding of this paper. In the North box, the soil-sink seasonal cycle peaks in July and August with a seasonal range of 18–21 Tg year^{-1} and posterior standard deviation of 8 Tg year^{-1}, and displays seasonality in agreement with current understanding of the moisture dependence of soil uptake in the Northern Hemisphere (Bertagni et al., 2021). The minimum occurs in January–February. There is reasonable agreement between the two methods of deriving chemical production. When deriving CH_2O from OH values, the peak occurs slightly later and with a slightly larger range compared to when CH_2O is also optimized. The range between all cases is primarily a result of the prior range of estimates on the CH_2O uncertainty, highlighting the importance of accurately modelling free tropospheric CH_2O for simulating the H_2 budget (see Fig. S7). The results provide a basis for testing the fidelity of land models for the seasonal phase in uptake of H_2 by soil in northern latitudes.

In the Tropics box, the retrieved soil sink shows smaller seasonal range compared to the North box. The largest range is retrieved in the CH_2O derived from the OH case at 8 Tg year^{-1} with a posterior standard deviation of 8 Tg year^{-1}, which peaks in July–August, similar to the North box. This is also the time of maximum variation between the three cases, which is partly driven by the time of maximum biomass burning that peaks in the Tropics box (see Fig. S8). The seasonality of the Tropics box soil sink agrees fairly well with the previous soil sink inversion by Bousquet et al. (2011).

In the South box, the smallest soil sink range is retrieved at 2–3 Tg year^{-1} with a posterior standard deviation of 2.5 Tg year^{-1}. The soil sink peaks in January–February and has a minimum in April for the 15 %, 35 %, and 55 % uncertainty cases and peaks in March and has a minimum in July for the CH_2O derived from OH. This is different than what was reported in some previous retrieval studies that show a peak loss in November (Bousquet et al., 2011; Xiao et al., 2007), but is in better agreement with others that show soil loss peaking in February (Rhee et al., 2006). One source of retrieval differences could be the choice of the box northern boundary at 20° S. For example, Xiao et al. (2007) used a 4-box model with a boundary at 30° S. The small South box seasonal range is expected due to there being significantly less land compared to the North and Tropics boxes.

The global H_2 soil sink yearly mean range retrieved is 26 Tg year^{-1} for the CH_2O derived from OH case and between 13 Tg year^{-1} and 23 Tg year^{-1} for the 15 %, 35 %, and 55 % uncertainty cases. All cases peak in July–August consistent with other observational and modelling studies (e.g. Bousquet et al., 2011; Brown et al., 2025b). The 35 % uncertainty and CH_2O derived from OH cases have a posterior standard deviation of 10 Tg year^{-1}.

The soil sinks yearly ranges and phases shown here are most consistent between the cases for the North and South boxes where the OH seasonal cycles retrieved from HFC-152a are most robust. Since the seasonal cycle of chemical production through CH_2O photolysis in this study is either strongly correlated to OH in the prior covariance or derived from retrieved OH using Eq. 1, and the seasonal cycle of emissions of H_2 are tied to biomass burning and anthropogenic seasonality, there is confidence in the retrieved phase of the

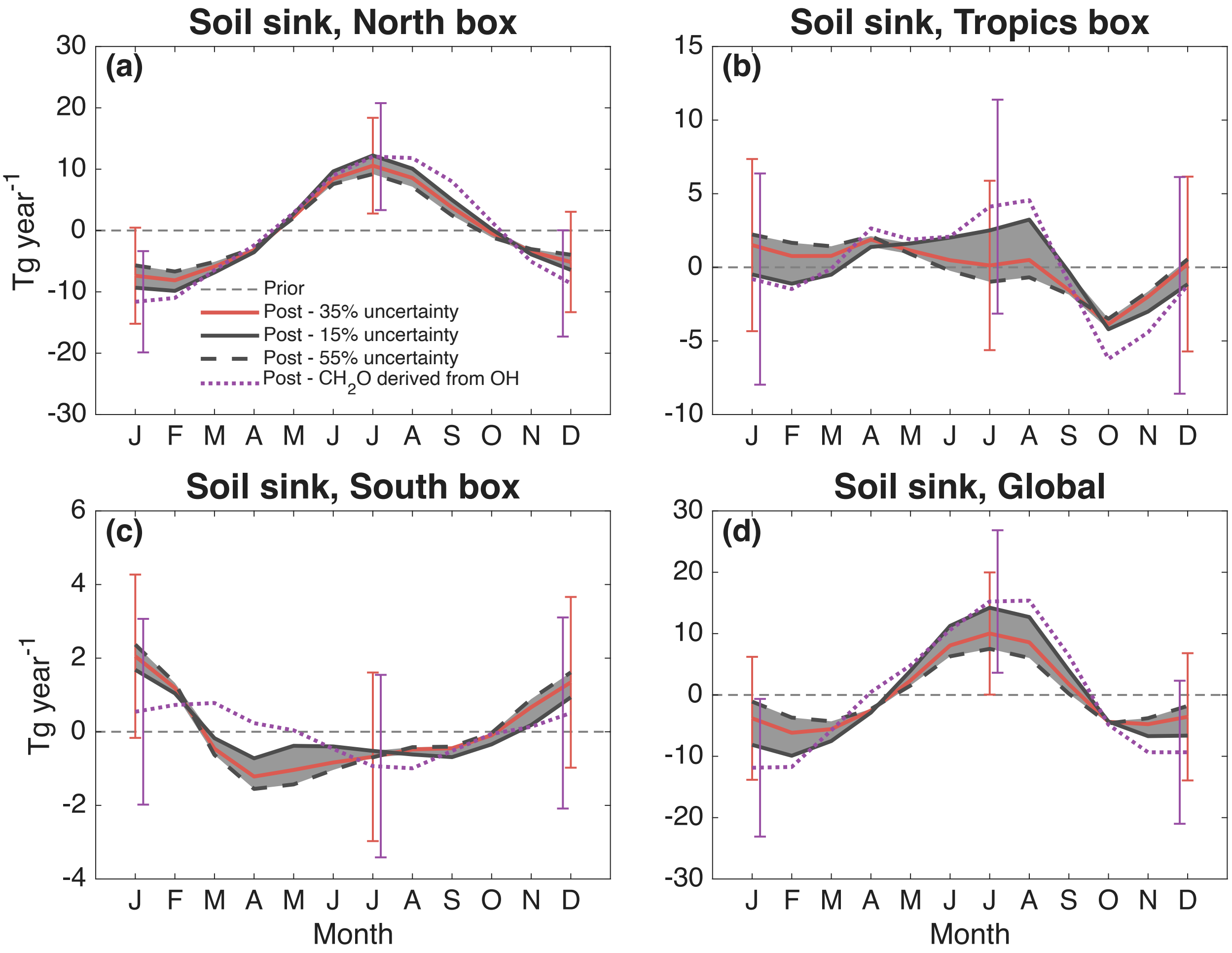

Figure 4. Monthly anomalies of the H_2 soil sink from the yearly mean for all cases in (a) the North box, (b) the Tropics box, (c) the South box, and (d) globally. The shaded region shows the range between the 15 %, 35 %, and 55 % uncertainty cases (see Table 1). The CH_2O derived from OH case (dotted line) is also shown. The error bars show the retrieved posterior standard deviation uncertainty for the 35 % uncertainty case and the CH_2O derived from OH case. The grey dashed line shows the prior estimate for the soil sink in each box. Results are averaged over the 2010–2022 time series.

https://doi.org/10.5194/egusphere-2025-6461
Preprint. Discussion started: 19 January 2026

soil sink. This is especially the case in the North box, South box, and globally (since the majority of the H_2 soil loss is occurring in the Northern Hemisphere). The Tropics box retrieved OH is more sensitive to initial OH and transport conditions (Fig. S2) and observed HFC-152a in the Tropics box shows much larger year-to-year variability in the seasonal cycle (Fig. 2). Therefore, confidence in the Tropics box retrieved soil sink phase is lower and is reflected in the differences in phase between the cases (Fig. 4b). The amplitude of the retrieved seasonal cycle is, however, dependent on the prior values for chemical production and H_2 emissions and is the reason for large prior uncertainties used, which results in large posterior uncertainty. However, the retrieved chemical production and H_2 emission anomalies are consistent among cases, with the largest differences between cases relative to the seasonal amplitude is seen in the Tropics box chemical production (see Figs. S7 and S8).

4 Conclusions

A three-box model inversion of OH concentration and the sources and sinks of H_2 is presented in this study, revealing seasonal changes in oxidative loss and soil uptake. The three-box model uses an equal mass tropospheric box model with the three boxes prescribed as: North (20°–90° N), Tropics (20° S–20° N), and South (90°–20° S).

The inversion uses a Bayesian optimal estimation of monthly resolved OH, the H_2 soil sink, H_2 chemical production through CH_2O photolysis, and H_2 emissions in the three boxes. Monthly information of HFC-152a and H_2 dry air mixing ratios from the Advanced Global Atmospheric Gas Experiment and the National Oceanic and the Atmospheric Administration global surface air sampling network are used to constrain the OH signal. This information is then used to infer the seasonal anomaly of H_2 oxidation in each box. Anomalies only, rather than absolute values, are analyzed because HFC-152a emissions are not well constrained, which limits the ability to retrieve accurate absolute OH values, which then in turn affects the absolute soil sink retrieval. The retrieval of the seasonal range and phase in the North and South boxes is however relatively independent of prior OH mean values and transport terms used between the boxes for the scenarios tested here. Due to the large correlations between H_2 sources and sinks, particularly OH loss and chemical production, and the uncertainties in H_2 emissions, three retrievals are conducted spanning a range of prior uncertainties for CH_2O photolysis and H_2 emissions of 15 %, 35 %, and 55 %. In these cases, prior OH uncertainty is cross correlated with chemical production, obtained from WACCM model simulations and TROPESS reanalysis. An additional case where H_2 chemical production is derived from retrieved OH data is performed using a pseudo-linear relationship between OH and CH_2O.

Between the two methods of retrieving H_2 chemical production, the retrieved OH is nearly identical due to the inclusion of HFC-152a data. The largest seasonal range of H_2 oxidative loss is retrieved in the North box at 8 Tg year^{-1}, compared to the South box of 7 Tg year^{-1}. The retrieved posterior standard deviation is 1 Tg year^{-1} for both the North and South boxes. The oxidative loss peaks in July in the North box and January in the South box.

The North box retrieved soil sink has a range of 18–21 Tg year^{-1} between the 4 cases that peaks in July–August with a posterior standard deviation of 8 Tg year^{-1}, while the South box has a much lower soil sink range of 2–3 Tg year^{-1} peaking in January–March between the four cases with a posterior standard deviation of 2.5 Tg year^{-1}. The OH and soil sink loss in the Tropics region is more consistent throughout the year but has larger uncertainty in both the phase and amplitude of the soil sink. Globally, there is consistency in the phase of the soil sink which peaks in July–August, however, there are larger differences between cases in the range compared to the North box of between 13–26 Tg year^{-1} with a posterior standard deviation of 10 Tg year^{-1}.

Retrieving OH through HFC-152a seasonality with inferred or correlated chemical production of H_2 gives confidence in the North and South box soil sink seasonal phase retrieved here. However, uncertainty in the seasonal range of the soil sink, reflected in the large posterior standard deviations is dependent on prior uncertainty in CH_2O and H_2 emissions. Therefore, further constraining the soil sink will require reducing these uncertainties. Nonetheless, the results presented here provide a useful tool for fully coupled land chemistry climate models to verify seasonal soil uptake when incorporating an interactive hydrogen scheme.

Code and data availability

The NOAA global network flask air H_2 measurements are available at https://doi.org/10.15138/WP0W-EZ08 (Pétron et al., 2025). The AGAGE data is available at http://doi.org/10.60718/75d7-qe84 (Prinn et al., 2025). EDGAR emissions data are available at http://doi:10.2760/9816914 (Crippa et al., 2025). TROPESS data is available at 10.5067/6F26QNSI0DNX (Miyazaki, 2024). WACCM data used in this study and the box model code and inversion can be found at https://doi.org/10.7910/DVN/T6V2DI (Stone, 2025).

Author contributions

KS and SS formulated the study, KS performed the analysis and wrote the manuscript, KS and CC developed the forward model, KS, SS, CC, LW, PK, GP, and JM engaged in discussions and edited the manuscript, PK, GP, JM, and SD provided the data.

Competing interests

The authors have no competing interests.

Acknowledgements

KS, CC, and SS gratefully acknowledge funding from the MIT Energy Initiative (MITEI), grant 2565489. AGAGE is supported principally by the National Aeronautics and Space Administration (USA) grants to the Massachusetts Institute of Technology and the Scripps Institution of Oceanography. In Australia, the Kennaook/Cape Grim operations were supported by the Commonwealth Scientific and Industrial Research Organization (CSIRO), the Bureau of Meteorology (Australia), the

Department of Climate Change, Energy, the Environment and Water (Australia), Refrigerant Reclaim Australia, the Australian Refrigeration Council and through the NASA award to MIT with subaward to CSIRO for Cape Grim (grant no. 80NSSC21K1369). The Department for Energy Security and Net Zero (DESNZ) in the United Kingdom supported the University of Bristol for operations at Mace Head, Ireland (contracts 1028/06/2015, 1537/06/2018 and 5488/11/2021) and through the NASA award to MIT with the subaward to University of Bristol for Mace Head and Barbados (grant no. 80NSSC21K1369). Operation of the American Samoa observatory (SMO) is funded by the National Oceanic and Atmospheric Administration (NOAA) in the USA. AGAGE operations at SMO as well as at the central calibration facility (HFC-152a) at Scripps Institution of Oceanography are funded by the National Aeronautics and Space Administration (NASA) in the USA. The NOAA cooperative global air sampling network is operated by the Global Monitoring Laboratory in Boulder, CO and it relies on its air sampling partners around the world. The NOAA flask air H_2 measurements are conducted at the GML and use the WMO H_2 calibration scale developed and maintained by the MPI-BGC (Jordan and Steinberg, 2011). GP was supported by NOAA Cooperative Agreement NA22OAR4320151 and by the U.S. Department of Energy's Office of Energy Efficiency and Renewable Energy (EERE) under the Hydrogen and Fuel Cell Technologies Office (HFTO).

References

Bertagni, M. B., Paulot, F., and Porporato, A.: Moisture Fluctuations Modulate Abiotic and Biotic Limitations of H_2 Soil Uptake, Glob. Biogeochem. Cycles, 35, https://doi.org/10.1029/2021gb006987, 2021.

Bertagni, M. B., Pacala, S. W., Paulot, F., and Porporato, A.: Risk of the hydrogen economy for atmospheric methane, Nat. Commun., 13, https://doi.org/10.1038/s41467-022-35419-7, 2022.

Bousquet, P., Hauglustaine, D. A., Peylin, P., Carouge, C., and Ciais, P.: Two decades of OH variability as inferred by an inversion of atmospheric transport and chemistry of methyl chloroform, Atmos Chem Phys, 5, 2635–2656, https://doi.org/10.5194/acp-5-2635-2005, 2005.

Bousquet, P., Yver, C., Pison, I., Li, Y. S., Fortems, A., Hauglustaine, D., Szopa, S., Rayner, P. J., Novelli, P., Langenfelds, R., Steele, P., Ramonet, M., Schmidt, M., Foster, P., Morfopoulos, C., and Ciais, P.: A three-dimensional synthesis inversion of the molecular hydrogen cycle: Sources and sinks budget and implications for the soil uptake, J. Geophys. Res., 116, D01302, https://doi.org/10.1029/2010JD014599, 2011.

Brown, M. A. J., Warwick, N. J., Abraham, N. L., Griffiths, P. T., Rumbold, S. T., Folberth, G. A., O'Connor, F. M., and Archibald, A. T.: Development of Fully Interactive Hydrogen with Methane in UKESM1.0, https://doi.org/10.5194/egusphere-2025-2676, 21 July 2025a.

Brown, M. A. J., Warwick, N. J., and Archibald, A. T.: Multi-Model Assessment of Future Hydrogen Soil Deposition and Lifetime Using CMIP6 Data, Geophys. Res. Lett., 52, e2024GL113653, https://doi.org/10.1029/2024GL113653, 2025b.

Burkholder, J., Hondnebrog, O., McDonald, B., Orkin, V., Papadimitriou, V., and Van Hoomissen, D.: SUMMARY OF ABUNDANCES, LIFETIMES, ODPs, REs, GWPs, GTPs, Scientific Assessment of Ozone Depletion 2022, 2023.

Burkholder, J. B., Sander, S. P., Abbatt, J., Barker, C. R., Cappa, C., Crounse, J. D., Dibble, T. S., Huie, R. E., Kolb, C. E., Kurylo, M. J., Orkin, V. L., Percival, C. J., Wilmouth, D. M., and Wine, P. H.: Chemical Kinetics and Photochemical Data for Use in Atmospheric Studies, Evaluation No. 19, JPL Publication 19-5, Jet Propulsion Laboratory, Pasadena, 2019.

Chen, C., Solomon, S., and Stone, K.: On the chemistry of the global warming potential of hydrogen, Front. Energy Res., 12, 1463450, https://doi.org/10.3389/fenrg.2024.1463450, 2024.

Conrad, R., Weber, M., and Weiler, W.: Kinetics and electron transport of soil hydrogenases catalyzing the oxidation of atmospheric hydrogen, Soil Biol. Biochem., 15, 167–173, https://doi.org/10.1016/0038-0717(83)90098-6, 1983.

Crippa, M., Guizzardi, D., Pagani, F., Banja, M., Muntean, M., Schaaf, E., Quadrelli, R., Risquez Martin, A., Taghavi-Moharamli, P., Köykkä, J., Grassi, G., Melo, J., Suárez-Moreno, M., Sedano, F., San-Miguel, J., Manca, G., Pisoni, E., Pekar, F., and European Commission (Eds.): GHG emissions of all world countries: 2025, Publications Office, Luxembourg, 1 pp., https://doi.org/10.2760/5917997, 2025.

Crutzen, P. J., Heidt, L. E., Krasnec, J. P., Pollock, W. H., and Seiler, W.: Biomass burning as a source of atmospheric gases CO, H2, N2O, NO, CH3CJ and COS, Nature, 282, 253–256, https://doi.org/10.1038/282253a0, 1979.

Cunnold, D. M., Fraser, P. J., Weiss, R. F., Prinn, R. G., Simmonds, P. G., Miller, B. R., Alyea, F. N., and Crawford, A. J.: Global trends and annual releases of CCl_3 F and CCl_2 F_2 estimated from ALE/GAGE and other measurements from July 1978 to June 1991, J. Geophys. Res. Atmospheres, 99, 1107–1126, https://doi.org/10.1029/93JD02715, 1994.

Derwent, R. G.: Global warming potential (GWP) for hydrogen: Sensitivities, uncertainties and meta-analysis, Int. J. Hydrog. Energy, 48, 8328–8341, https://doi.org/10.1016/j.ijhydene.2022.11.219, 2023.

Duncan, B. N., Martin, R. V., Staudt, A. C., Yevich, R., and Logan, J. A.: Interannual and seasonal variability of biomass burning emissions constrained by satellite observations, J. Geophys. Res. Atmospheres, 108, https://doi.org/10.1029/2002JD002378, 2003.

Ehhalt, D. H. and Rohrer, F.: The tropospheric cycle of H_2: a critical review, Tellus B Chem. Phys. Meteorol., 61, 500, https://doi.org/10.1111/j.1600-0889.2009.00416.x, 2009.

Ehhalt, D. H. and Rohrer, F.: Deposition velocity of H_2: a new algorithm for its dependence on soil moisture and temperature, Tellus B Chem. Phys. Meteorol., 65, 19904, https://doi.org/10.3402/tellusb.v65i0.19904, 2013.

Esquivel-Elizondo, S., Hormaza Mejia, A., Sun, T., Shrestha, E., Hamburg, S. P., and Ocko, I. B.: Wide range in estimates of hydrogen emissions from infrastructure, Front. Energy Res., 11, 1207208, https://doi.org/10.3389/fenrg.2023.1207208, 2023.

Feng, L., Smith, S. J., Braun, C., Crippa, M., Gidden, M. J., Hoesly, R., Klimont, Z., Van Marle, M., Van Den Berg, M., and Van Der Werf, G. R.: The generation of gridded emissions data for CMIP6, Geosci. Model Dev., 13, 461–482, https://doi.org/10.5194/gmd-13-461-2020, 2020.

Gettelman, A., Mills, M. J., Kinnison, D. E., Garcia, R. R., Smith, A. K., Marsh, D. R., Tilmes, S., Vitt, F., Bardeen, C. G., McInerny, J., Liu, H. -L., Solomon, S. C., Polvani, L. M., Emmons, L. K., Lamarque, J. -F., Richter, J. H., Glanville, A. S., Bacmeister, J. T., Phillips, A. S., Neale, R. B., Simpson, I. R., DuVivier, A. K., Hodzic, A., and

Randel, W. J.: The Whole Atmosphere Community Climate Model Version 6 (WACCM6), J. Geophys. Res. Atmospheres, 124, 12380–12403, https://doi.org/10.1029/2019JD030943, 2019.

Hauglustaine, D. A. and Ehhalt, D. H.: A three-dimensional model of molecular hydrogen in the troposphere, J. Geophys. Res. Atmospheres, 107, https://doi.org/10.1029/2001jd001156, 2002.

Hersbach, H., Bell, B., Berrisford, P., Hirahara, S., Horányi, A., Muñoz-Sabater, J., Nicolas, J., Peubey, C., Radu, R., Schepers, D., Simmons, A., Soci, C., Abdalla, S., Abellan, X., Balsamo, G., Bechtold, P., Biavati, G., Bidlot, J., Bonavita, M., Chiara, G., Dahlgren, P., Dee, D., Diamantakis, M., Dragani, R., Flemming, J., Forbes, R., Fuentes, M., Geer, A., Haimberger, L., Healy, S., Hogan, R. J., Hólm, E., Janisková, M., Keeley, S., Laloyaux, P., Lopez, P., Lupu, C., Radnoti, G., Rosnay, P., Rozum, I., Vamborg, F., Villaume, S., and Thépaut, J.: The ERA5 Global Reanalysis, Q. J. R. Meteorol. Soc., https://doi.org/10.1002/qj.3803, 2020.

Hoesly, R., Smith, S., Ahsan, H., Prime, N., O'Rourke, P., Crippa, M., Klimont, Z., Guizzardi, D., Feng, L., Harkins, C., MCDONALD, B., and Wang, S.: CEDS v_2025_04_18 Gridded Emissions Data 0.5 degree [dataset] (v_2025_03_18), https://doi.org/10.5281/ZENODO.15127477, 2025.

Hydrogen Council: Path to hydrogen competitiveness: A cost perspective, https://hydrogencouncil.com/en/path-to-hydrogen-competitiveness-a-cost-perspective/, 2020.

IEA: Global Hydrogen Review 2023, Paris, https://www.iea.org/reports/global-hydrogen-review-2023, 2023.

Jordan, A. and Steinberg, B.: Calibration of atmospheric hydrogen measurements, Atmospheric Meas. Tech., 4, 509–521, https://doi.org/10.5194/amt-4-509-2011, 2011.

Ko, M. K. W., Newman, P. A., Reimann, S., and Strahan, S. E.: Lifetimes of Stratospheric Ozone-Depleting Substances, Their Replacements and Related Species, SPARC Rep. No 6 WCRP-152013, 2013.

Lawrence, M. G. and Jockel, P.: What does the global mean OH concentration tell us?, Atmos Chem Phys, 1, 37–49, https://doi.org/10.5194/acp-1-37-2001, 2001.

Liang, Q., Chipperfield, M. P., Fleming, E. L., Abraham, N. L., Braesicke, P., Burkholder, J. B., Daniel, J. S., Dhomse, S., Fraser, P. J., Hardiman, S. C., Jackman, C. H., Kinnison, D. E., Krummel, P. B., Montzka, S. A., Morgenstern, O., McCulloch, A., Mühle, J., Newman, P. A., Orkin, V. L., Pitari, G., Prinn, R. G., Rigby, M., Rozanov, E., Stenke, A., Tummon, F., Velders, G. J. M., Visioni, D., and Weiss, R. F.: Deriving Global OH Abundance and Atmospheric Lifetimes for Long-Lived Gases: A Search for CH_3 CCl_3 Alternatives, J. Geophys. Res. Atmospheres, 122, https://doi.org/10.1002/2017JD026926, 2017.

van Marle, M. J. E., Kloster, S., Magi, B. I., Marlon, J. R., Daniau, A. L., Field, R. D., Arneth, A., Forrest, M., Hantson, S., Kehrwald, N. M., Knorr, W., Lasslop, G., Li, F., Mangeon, S., Yue, C., Kaiser, J. W., and Van Der Werf, G. R.: Historic global biomass burning emissions for CMIP6 (BB4CMIP) based on merging satellite observations with proxies and fire models (1750-2015), Geosci. Model Dev., 10, 3329–3357, https://doi.org/10.5194/gmd-10-3329-2017, 2017.

van Marle, M. and Werf, G. van der: input4MIPs.CMIP7.DRES.DRES-CMIP-BB4CMIP7-2-0 [dataset], https://doi.org/10.25981/ESGF.INPUT4MIPS.CMIP7/2524040, 2025.

Miyazaki, K.: TROPESS Chemical Reanalysis CH2O Monthly 3-dimensional Product, [Dataset], https://doi.org/10.5067/6F26QNSI0DNX, 2024.

Miyazaki, K., Bowman, K., Sekiya, T., Eskes, H., Boersma, F., Worden, H., Livesey, N., Payne, V. H., Sudo, K., Kanaya, Y., Takigawa, M., and Ogochi, K.: Updated tropospheric chemistry reanalysis and emission estimates, TCR-2, for 2005–2018, Earth Syst. Sci. Data, 12, 2223–2259, https://doi.org/10.5194/essd-12-2223-2020, 2020.

Montzka, S. A., Krol, M., Dlugokencky, E., Hall, B., Jöckel, P., and Lelieveld, J.: Small Interannual Variability of Global Atmospheric Hydroxyl, Science, 331, 67–69, https://doi.org/10.1126/science.1197640, 2011.

Naus, S., Montzka, S. A., Patra, P. K., and Krol, M. C.: A three-dimensional-model inversion of methyl chloroform to constrain the atmospheric oxidative capacity, Atmospheric Chem. Phys., 21, 4809–4824, https://doi.org/10.5194/acp-21-4809-2021, 2021.

Novelli, P. C., Lang, P. M., Masarie, K. A., Hurst, D. F., Myers, R., and Elkins, J. W.: Molecular hydrogen in the troposphere: Global distribution and budget, J. Geophys. Res. Atmospheres, 104, 30427–30444, https://doi.org/10.1029/1999JD900788, 1999.

Ouyang, Z., Jackson, B. J., Saunois, M., and Canadell, J. G.: The global hydrogen budget, Nature, https://doi.org/10.1038/s41586-025-09806-1, 2025a.

Ouyang, Z., Jackson, R. B., Saunois, M., Canadell, J. G., Zhao, Y., Morfopoulos, C., Krummel, P. B., Patra, P. K., Peters, G. P., Dennison, F., Gasser, T., Archibald, A. T., Arora, V., Baudoin, G., Chandra, N., Ciais, P., Davis, S. J., Feron, S., Guo, F., Hauglustaine, D., Jones, C. D., Jones, M. W., Kato, E., Kennedy, D., Knauer, J., Lienert, S., Lombardozzi, D., Melton, J. R., Nabel, J. E. M. S., O'Sullivan, M., Pétron, G., Poulter, B., Rogelj, J., Sandoval Calle, D., Smith, P., Suntharalingam, P., Tian, H., Wang, C., and Wiltshire, A.: The global hydrogen budget, Nature, 648, 616–624, https://doi.org/10.1038/s41586-025-09806-1, 2025b.

Patra, P. K., Krol, M. C., Prinn, R. G., Takigawa, M., Mühle, J., Montzka, S. A., Lal, S., Yamashita, Y., Naus, S., Chandra, N., Weiss, R. F., Krummel, P. B., Fraser, P. J., O'Doherty, S., and Elkins, J. W.: Methyl Chloroform Continues to Constrain the Hydroxyl (OH) Variability in the Troposphere, J. Geophys. Res. Atmospheres, 126, e2020JD033862, https://doi.org/10.1029/2020JD033862, 2021.

Paulot, F., Paynter, D., Naik, V., Malyshev, S., Menzel, R., and Horowitz, L. W.: Global modeling of hydrogen using GFDL-AM4.1: Sensitivity of soil removal and radiative forcing, Int. J. Hydrog. Energy, 46, 13446–13460, https://doi.org/10.1016/j.ijhydene.2021.01.088, 2021.

Paulot, F., Pétron, G., Crotwell, A., Crotwell, M., Handley, P., Kofler, J., Madronich, M., Mefford, T., Moglia, E., Mund, J., Thoning, K., Biraud, S. C., and Andrews, A.: Imprint of Anthropogenic Sources and Soil Removal on the Surface Concentration of H_2 in the Contiguous US, Environ. Sci. Technol., 59, 25214–25224, https://doi.org/10.1021/acs.est.5c04607, 2025.

Pétron, G., Crotwell, A. M., Mund, J., Crotwell, M., Mefford, T., Thoning, K., Hall, B., Kitzis, D., Madronich, M., Moglia, E., Neff, D., Wolter, S., Jordan, A., Krummel, P., Langenfelds, R., and Patterson, J.: Atmospheric H_2 observations from the NOAA Cooperative Global Air Sampling Network, Atmospheric Meas. Tech., 17, 4803–4823, https://doi.org/10.5194/amt-17-4803-2024, 2024.

Pétron, G., Lan, X., Baugh, K., Crotwell, A. M., Crotwell, M. J., DeVogel, S., Madronich, M., Mauss, J., Mefford, T., Moglia, E., Morris, S., Mund, J. W., Searle, A., Thoning, K. W., Wolter, S., and Miller, J.: Atmospheric Hydrogen Dry Air Mole Fractions from the NOAA GML Global Greenhouse Gas Reference Network, Carbon Cycle Cooperative Global Air Sampling Network: 2009 - Present (2025-09-30), https://doi.org/10.15138/WP0W-EZ08, 2025.

Pieterse, G., Krol, M. C., Batenburg, A. M., M. Brenninkmeijer, C. A., Popa, M. E., O'Doherty, S., Grant, A., Steele, L. P., Krummel, P. B., Langenfelds, R. L., Wang, H. J., Vermeulen, A. T., Schmidt, M., Yver, C., Jordan, A., Engel, A., Fisher, R. E., Lowry, D., Nisbet, E. G., Reimann, S., Vollmer, M. K., Steinbacher, M., Hammer, S., Forster, G., Sturges, W. T., and Röckmann, T.: Reassessing the variability in atmospheric H_2 using the two-way nested TM5 model, J. Geophys. Res. Atmospheres, 118, 3764–3780, https://doi.org/10.1002/jgrd.50204, 2013.

Prinn, R., Cunnold, D., Simmonds, P., Alyea, F., Boldi, R., Crawford, A., Fraser, P., Gutzler, D., Hartley, D., Rosen, R., and Rasmussen, R.: Global average concentration and trend for hydroxyl radicals deduced from ALE/GAGE trichloroethane (methyl chloroform) data for 1978–1990, J. Geophys. Res. Atmospheres, 97, 2445–2461, https://doi.org/10.1029/91JD02755, 1992.

Prinn, R., Weiss, R., Arduini, J., Choi, H., Engel, A., Fraser, P., Ganesan, A., Harth, C., Hermansen, O., Kim, J., Krummel, P., Loh, Z., Lunder, C., Maione, M., Manning, A., Mitrevski, B., Mühle, J., O'Doherty, S., Park, S., Pitt, J., Reimann, S., Rigby, M., Saito, T., Salameh, P., Schmidt, R., Simmonds, P., Stanley, K., Stavert, A., Steele, P., Vollmer, M., Wagenhäuser, T., Wang, H., Wenger, A., Western, L., Yao, B., Young, D., Zhou, L., and Zhu, L.: The dataset of in-situ measurements of chemically and radiatively important atmospheric gases from the Advanced Global Atmospheric Gas Experiment (AGAGE) and affiliated stations (20250721), https://doi.org/10.60718/75D7-QE84, 2025.

Prinn, R. G., Weiss, R. F., Arduini, J., Arnold, T., DeWitt, H. L., Fraser, P. J., Ganesan, A. L., Gasore, J., Harth, C. M., Hermansen, O., Kim, J., Krummel, P. B., Li, S., Loh, Z. M., Lunder, C. R., Maione, M., Manning, A. J., Miller, B. R., Mitrevski, B., Mühle, J., O'Doherty, S., Park, S., Reimann, S., Rigby, M., Saito, T., Salameh, P. K., Schmidt, R., Simmonds, P. G., Steele, L. P., Vollmer, M. K., Wang, R. H., Yao, B., Yokouchi, Y., Young, D., and Zhou, L.: History of chemically and radiatively important atmospheric gases from the Advanced Global Atmospheric Gases Experiment (AGAGE), Earth Syst. Sci. Data, 10, 985–1018, https://doi.org/10.5194/essd-10-985-2018, 2018.

Reji, L., Bertagni, M. B., Paulot, F., Qin, Q., and Zhang, X.: Global implications of a low soil moisture threshold for microbial hydrogen uptake, Nat. Commun., https://doi.org/10.1038/s41467-025-67208-3, 2025.

Rhee, T. S., Brenninkmeijer, C. A. M., and Rockmann, T.: The overwhelming role of soils in the global atmospheric hydrogen cycle, Atmos Chem Phys, 6, 1611–1625, https://doi.org/10.5194/acp-6-1611-2006, 2006.

Rodgers, C. D.: Inverse methods for atmospheric sounding, World Scientific, Singapore, https://doi.org/10.1142/3171, 2000.

Sand, M., Skeie, R. B., Sandstad, M., Krishnan, S., Myhre, G., Bryant, H., Derwent, R., Hauglustaine, D., Paulot, F., Prather, M., and Stevenson, D.: A multi-model assessment of the Global Warming Potential of hydrogen, Commun. Earth Environ., 4, 203, https://doi.org/10.1038/s43247-023-00857-8, 2023.

Sanderson, M. G., Collins, W. J., Derwent, R. G., and Johnson, C. E.: Simulation of Global Hydrogen Levels Using a Lagrangian Three-Dimensional Model, J. Atmospheric Chem., 46, 15–28, https://doi.org/10.1023/A:1024824223232, 2003.

Simmonds, P. G., Rigby, M., Manning, A. J., Lunt, M. F., O'Doherty, S., McCulloch, A., Fraser, P. J., Henne, S., Vollmer, M. K., Mühle, J., Weiss, R. F., Salameh, P. K., Young, D., Reimann, S., Wenger, A., Arnold, T., Harth, C. M., Krummel, P. B., Steele, L. P., Dunse, B. L., Miller, B. R., Lunder, C. R., Hermansen, O., Schmidbauer, N., Saito, T., Yokouchi, Y., Park, S., Li, S., Yao, B., Zhou, L. X., Arduini, J., Maione, M., Wang, R. H. J., Ivy, D., and Prinn, R. G.: Global and regional emissions estimates of 1,1-difluoroethane (HFC-152a, CH_3 CHF_2) from in situ and air archive observations, Atmospheric Chem. Phys., 16, 365–382, https://doi.org/10.5194/acp-16-365-2016, 2016.

Spivakovsky, C. M., Logan, J. A., Montzka, S. A., Balkanski, Y. J., Foreman-Fowler, M., Jones, D. B. A., Horowitz, L. W., Fusco, A. C., Brenninkmeijer, C. A. M., Prather, M. J., Wofsy, S. C., and McElroy, M. B.: Three-dimensional climatological distribution of tropospheric OH: Update and evaluation, J. Geophys. Res. Atmospheres, 105, 8931–8980, https://doi.org/10.1029/1999JD901006, 2000.

Stone, K. A.: Data and code for paper titled: "Constraining the atmospheric hydrogen oxidation and soil sinks using HFC-152a" [Code and Dataset] (1.0), https://doi.org/10.7910/DVN/T6V2DI, 2025.

Thompson, R. L., Montzka, S. A., Vollmer, M. K., Arduini, J., Crotwell, M., Krummel, P. B., Lunder, C., Mühle, J., O'Doherty, S., Prinn, R. G., Reimann, S., Vimont, I., Wang, H., Weiss, R. F., and Young, D.: Estimation of the atmospheric hydroxyl radical oxidative capacity using multiple hydrofluorocarbons (HFCs), Atmospheric Chem. Phys., 24, 1415–1427, https://doi.org/10.5194/acp-24-1415-2024, 2024.

Warwick, N. J., Archibald, A. T., Griffiths, P. T., Keeble, J., O'Connor, F. M., Pyle, J. A., and Shine, K. P.: Atmospheric composition and climate impacts of a future hydrogen economy, Atmospheric Chem. Phys., 23, 13451–13467, https://doi.org/10.5194/acp-23-13451-2023, 2023.

Western, L. M., Rigby, M., Mühle, J., Krummel, P. B., Lunder, C. R., O'Doherty, S., Reimann, S., Vollmer, M. K., Young, D., Adam, B., Fraser, P. J., Ganesan, A. L., Harth, C. M., Hermansen, O., Kim, J., Langenfelds, R. L., Loh, Z. M., Mitrevski, B., Pitt, J. R., Salameh, P. K., Schmidt, R., Stanley, K., Stavert, A. R., Wang, H.-J., Weiss, R. F., and Prinn, R. G.: Global emissions and abundances of chemically and radiatively important trace gases from the AGAGE network, Earth Syst. Sci. Data, 17, 6557–6582, https://doi.org/10.5194/essd-17-6557-2025, 2025.

Wolfe, G. M., Nicely, J. M., St. Clair, J. M., Hanisco, T. F., Liao, J., Oman, L. D., Brune, W. B., Miller, D., Thames, A., González Abad, G., Ryerson, T. B., Thompson, C. R., Peischl, J., McKain, K., Sweeney, C., Wennberg, P. O., Kim, M., Crounse, J. D., Hall, S. R., Ullmann, K., Diskin, G., Bui, P., Chang, C., and Dean-Day, J.: Mapping hydroxyl variability throughout the global remote troposphere via synthesis of airborne and satellite formaldehyde observations, Proc. Natl. Acad. Sci., 116, 11171–11180, https://doi.org/10.1073/pnas.1821661116, 2019.

Xiao, X., Prinn, R. G., Simmonds, P. G., Steele, L. P., Novelli, P. C., Huang, J., Langenfelds, R. L., O'Doherty, S., Krummel, P. B., Fraser, P. J., Porter, L. W., Weiss, R. F., Salameh, P., and Wang, R. H. J.: Optimal estimation of the soil uptake rate of molecular hydrogen from the Advanced Global Atmospheric Gases Experiment and other measurements, J. Geophys. Res. Atmospheres, 112, 2006JD007241, https://doi.org/10.1029/2006JD007241, 2007.

Yang, L. H., Jacob, D. J., Lin, H., Dang, R., Bates, K. H., East, J. D., Travis, K. R., Pendergrass, D. C., and Murray, L. T.: Assessment of Hydrogen's Climate Impact Is Affected by Model OH Biases, Geophys. Res. Lett., 52, e2024GL112445, https://doi.org/10.1029/2024GL112445, 2025.

Yashiro, H., Sudo, K., Yonemura, S., and Takigawa, M.: The impact of soil uptake on the global distribution of molecular hydrogen: chemical transport model simulation, Atmospheric Chem. Phys., 11, 6701–6719, https://doi.org/10.5194/acp-11-6701-2011, 2011.

Yonemura, S., Kawashima, S., and Tsuruta, H.: Continuous measurements of CO and H2 deposition velocities onto an andisol: uptake control by soil moisture, Tellus B, 51, 688–700, https://doi.org/10.1034/j.1600-0889.1999.t01-2-00009.x, 1999.